# Optical redshift and blueshift spectra in monolayer $\beta_{12}$-borophene: Inversion symmetry breaking effects

Le T. T. Phuong,[1,*] Bui D. Hoi,[1,†] and Mohsen Yarmohammadi[2,‡]
[1]*Faculty of Physics, University of Education, Hue University, Hue 530000, Viet Nam*
[2]*Department of Physics, The University of Texas at Dallas, Richardson, Texas 75080, USA*

(Received 18 May 2022; accepted 31 October 2022; published 9 November 2022)

We have calculated the optical conductivity of monolayer $\beta_{12}$-borophene in the presence of an inversion symmetry breaking (ISB) field. We theoretically formulate such a field to effectively be induced by a substrate through an orbital hybridization effect in the experimental growth process. In the electronic band structure, the effect of the ISB field on the anisotropic dispersion appears as a perturbed manipulation of the energy scale. Different orientations of dispersion of triplet and Dirac fermions in $\beta_{12}$-borophene cause anisotropic optical interband transitions. Simulated ISB-induced optical conductivity using the Kubo formula produces various optical redshift and blueshift spectra. The longitudinal (Hall) component of optical conductivity presents a pure redshift (blueshift) spectrum with the ISB field, whereas the coexistence of both redshift and blueshift spectra emerge for the transverse component. This paper is a handful for practical applications in two-dimensional-based optoelectronic devices.

DOI: 10.1103/PhysRevB.106.195409

## I. INTRODUCTION

After the discovery of graphene [1] the fabrication of two-dimensional (2D) materials was a way to create a better semiconductor industry. However, scientists continued to search both experimentally and theoretically novel 2D materials due to massless fermions in graphene which cause serious problems for practical applications [2]. Accordingly, silicene [3,4], germanene [3,5], and stanene [3,6,7] were successfully found. Later on, the reports on further 2D materials, such as the molybdenum disulfide [8], aluminene [9], arsenene [10], antimonene [11], bismuthene [12], and phosphorene [13–15] were published.

In the mid-1990s, a 2D graphenelike boron sheet—borophene—was first predicted by theory [16]. From 2005 to 2015, it was reported that borophene on a single-crystal Ag(111) substrate can also be formed [17–23]. The synthesized structures exhibited various planar and corrugated metallic phases associated with a strong anisotropy, which results in anisotropic electrical, magnetical, thermal, and optical properties [24]. Less number of electrons in the valence shell of boron atoms in borophene compared to those of carbon atoms in graphene makes it usually unstable, however, this can be resolved by increasing the number of boron atoms [17,18]. Borophene has recently attracted much attention because of its capability in practical applications. For instance, Mortazavi and co-workers [25,26] have shown that borophene films can act as anode materials with ultrahigh capacities which are required for designing high capacity and lightweight advanced rechargeable ion batteries. Also, it has been proven that the $\beta_{12}$- and $\chi_3$-borophene satisfy the basic requirements for Li-ion and Na-ion batteries [27].

Borophene is realized by introducing periodic boron atoms in a honeycomblike lattice. Depending on the arrangements of the extra boron atoms for the stabilization of the borophene structure, various monolayer-boron structures can be proposed. As it has been mentioned, recently, several monolayer boron phases have been experimentally realized. According to the results of Refs. [22,23,28,29], it was predicted that $\beta_{12}$-borophene is thermodynamically the most stable allotrope of borophene since the boron atoms in this phase weakly interact with the silver atoms of the Ag(111) substrate. For this reason, this type of borophene is considered here to make sure the theoretical predictions, and results can be experimentally observed. Another phase of borophene, $\chi_3$-borophene, has one atom less than $\beta_{12}$-borophene in its unit cell can also be stable on a substrate, but here we would continue with the most stable $\beta_{12}$-borophene phase.

The coexistence of triplet (three bands far from the zero Fermi level touch each other at the same momenta) and Dirac (two bands at the Fermi level touch each other at the same momenta) fermions in the electronic band structure of $\beta_{12}$-borophene makes it more interesting [17–21,30,31]. The electronic band structure of this phase contains a strong inversion symmetry, however, the practical application of borophene is limited due to its inherent metallic phase. The inversion symmetry plays an important role in this limitation. Therefore, one needs a powerful strategy to overcome this limitation. For example, for the metallic phase, our previous works [32–35] have reported that an external perpendicular electric field can open a gap in $\beta_{12}$-borophene and can form an electron- or hole-doped semiconducting phase. But, one still needs to propose a way to break the strong inversion symmetry such that one can find other physical aspects of the system for practical targets.

*lttphuong@hueuni.edu.vn
†Corresponding author: buidinhhoi@hueuni.edu.vn
‡mohsen.yarmohammadi@utdallas.edu

 

The by now reported novel physical insights of $\beta_{12}$-borophene are mostly focused on the electronic properties, whereas one finds a few theoretical works on the optical properties of $\beta_{12}$-borophene. Recently, it has been reported that the optical absorption coefficient of $\beta_{12}$-borophene can be engineered with the mechanical strain [36]. In another work by Lherbier *et al.* [37], optical and electronic properties of pristine and oxidized borophene have been investigated by first-principles approaches, and it has been found that the optical response of borophene can be strongly affected by oxidation, suggesting that optical measurements can serve as an efficient probe for borophene surface contamination. Furthermore, by investigating the electronic structure and bonding characteristics of borophene with the help of first-principles calculations, it has been reported that the optical properties of borophene exhibit strong anisotropy [38]. The effect of strain and surface functionalization on the optical responses of borophene has also been studied by employing *ab initio* techniques [39].

Finding optical transitions at low-frequency regime—redshift—and high-frequency regime of light—blueshift—is one of the most important optical features of material for practical optoelectronic applications, such as solar cells. In this paper, we focus on such a study in $\beta_{12}$-borophene by proposing an inversion symmetry breaking (ISB) field which can introduce the coexisted redshift and blueshift spectra. We model the system in the low-energy approximation to tune the behavior of optical conductivity via such a field. We find that optical transitions show these shifts anisotropically.

The paper is organized as follows. In Sec. II, we present the theoretical background for the five-band tight-binding Hamiltonian model of $\beta_{12}$-borophene. Section III presents the optical conductivity tensor in the absence and presence of an ISB field. The numerical results of pristine and ISB field-induced anisotropic optoelectronic features will be discussed in Sec. IV. Conclusions are given in Sec. V.

## II. HAMILTONIAN MODEL

As mentioned before, $\beta_{12}$-borophene is built of the boron atoms in a honeycomb lattice. In contrast to two carbon atoms in a unit cell of graphene, it contains five atoms in a unit cell with the bond length of $a \simeq 2.926$ Å [27,30,31]. These five atoms show an inversion symmetry property, see Fig. 1. Similar to the out-of-plane $\pi$ orbitals in graphene in the vicinity of zero Fermi energy, $\pi$ orbitals of boron atoms are also responsible for the effective Hamiltonian of both triplet and Dirac fermions in $\beta_{12}$-borophene, whereas $\sigma$ orbitals contribute to the in-plane covalent bonding [30]. Thus, we are allowed to use the $p_z$ basis of boron atoms.

In order to describe the behavior of fermions in the momentum space $\vec{k} = (k_x, k_y)$, one can define the structure factors $f_{\vec{k}} = e^{ik_y a/2\sqrt{3}}$ and $g_{\vec{k}} = 2e^{ik_y a/2\sqrt{3}} \cos(k_x a/2)$ for the following Hamiltonian [30,31]:

$$\hat{\mathcal{H}}(\vec{k}) = \begin{pmatrix} \varepsilon_a & t_{ab} g_{\vec{k}} & t_{ac} f^*_{\vec{k}} & 0 & t_{ae} f_{\vec{k}} \\ t_{ab} g^*_{\vec{k}} & \varepsilon_b & t_{bc} g_{\vec{k}} & t_{bd} f^*_{\vec{k}} & 0 \\ t_{ac} f_{\vec{k}} & t_{bc} g^*_{\vec{k}} & \varepsilon_c & t_{cd} g_{\vec{k}} & t_{ce} f^*_{\vec{k}} \\ 0 & t_{bd} f_{\vec{k}} & t_{dc} g^*_{\vec{k}} & \varepsilon_d & t_{de} g_{\vec{k}} \\ t_{ae} f^*_{\vec{k}} & 0 & t_{ce} f_{\vec{k}} & t_{de} g^*_{\vec{k}} & \varepsilon_e \end{pmatrix}. \quad (1)$$

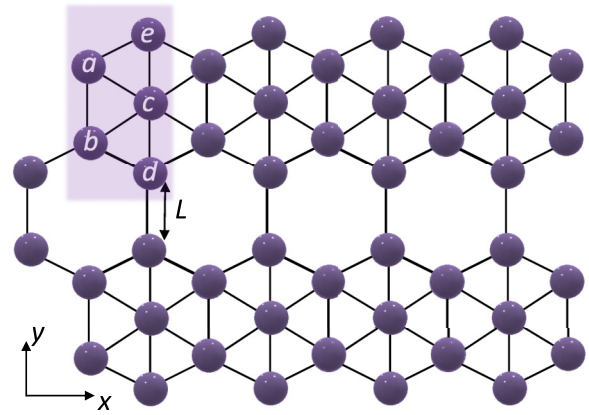


FIG. 1. The honeycomb lattice of $\beta_{12}$-borophene including five atoms $\{a, b, c, d, e\}$ in a unit cell (shaded rectangle). The lattice constant (bond length) between boron atoms is $L \simeq 2.926$ Å [27,30,31].

The on-site and hopping energies, respectively, $\varepsilon_j$ and $t_{jk}$ for $\{j, k\} = \{a, b, c, d, e\}$ can be obtained from first-principles calculations [31] by considering the inversion symmetry feature of the atoms, see Table I.

The proposition for an ISB effect is characterized by a field applied to the surface of $\beta_{12}$-borophene along the $z$ axis because the Hamiltonian used in our model is only valid for $p_z$ orbitals. So, to effectively affect these orbitals, we aim at applying the field only along the $z$ direction which, in turn, results in perturbing the pristine orbital hybridization of the system. The ISB field tries to break the inversion symmetry between the hopping energies, which can be understood from the perturbed orbital hybridization of the system. As shown in the left panel of Fig. 2, the inversion symmetry in the pristine $\beta_{12}$-borophene contains identical hopping energies between $\{a, b\}$ and $\{d, e\}$ atoms shown by blue double arrow, between $\{a, c\}$ and $\{c, e\}$ atoms shown by a yellow double arrow, and between $\{b, c\}$ and $\{c, d\}$ atoms shown by a green double arrow. However, here we aim at breaking these symmetries such that the hopping energies between atoms are not identical anymore as presented in the right panel of Fig. 2. Our scenario to do so is close to the one for orbital hybridization between the top and bottom surfaces of 2D topological insulators [40,41] where the effective hybridized states between their top and bottom surfaces are introduced by $\mathcal{A}\sigma_0 \otimes \tau_x$, where $\tau_x$ refers to the Pauli matrix in the surface space, whereas $\sigma_0$ is an identity matrix. In this term, the tunneling parameter $\mathcal{A}$ depends on the thickness of the topological insulator thin film. This is just a real example to understand our ISB field in the following.

Let us just consider a field that is exactly similar to the hybridized field above-mentioned. In analogy to the 2D

TABLE I. The effective inversion symmetrical on-site and hopping energies (in units of eV) of $\beta_{12}$-borophene [31]. Note that we have the following relations due to the inversion symmetry property of the lattice: $\varepsilon_a = \varepsilon_e$, $\varepsilon_b = \varepsilon_d$, $t_{ab} = t_{de}$, $t_{ac} = t_{ce}$, and $t_{bc} = t_{cd}$.

| $\varepsilon_a$ | $\varepsilon_b$ | $\varepsilon_c$ | $t_{ab}$ | $t_{ac}$ | $t_{bc}$ | $t_{bd}$ | $t_{ae}$ |
|---|---|---|---|---|---|---|---|
| +0.196 | −0.058 | −0.845 | −2.04 | −1.79 | −1.84 | −1.91 | −2.12 |

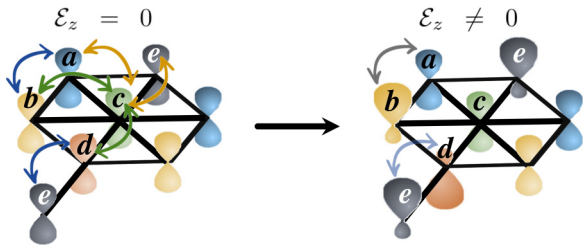


FIG. 2. Schematic of $p_z$ orbitals of five atoms $\{a, b, c, d, e\}$ in a unit cell of $\beta_{12}$-borophene in the absence and presence of ISB field $\mathcal{E}_z$.

topological insulators, we try to break the inversion symmetry between $\{a, b\}$ and $\{d, e\}$ atoms in $\beta_{12}$-borophene with the individual field $\mathcal{E}_z\tau_0 \otimes \eta_x$, where $\tau_0$ is the identity matrix and $\eta_x$ is the $x$ component of the Pauli matrix in the atomic space. It is worth noting that this is only acting on four atoms $\{a, b, d, e\}$. This field is tuning the orbital distribution of atoms on the top and bottom sides of 2D $\beta_{12}$-borophene. This tuning can be performed by a substrate with different atoms to induce different potentials into the hopping energies. For example, in a very recent work [42], it has been shown that the interfacial charge transfer doping can affect the electronic properties of $\beta_{12}$-borophene. Although this reference is not a direct observation of our ISB field, it confirms the availability of extra potentials induced to the boron atoms through various substrates, which will certainly break the inversion symmetry. As for the direction of the field, we would argue that in the term $\mathcal{E}_z\tau_0 \otimes \eta_x$ the sign of $\mathcal{E}_z$ is not important for $\{\pi, -\pi\}$-orbital hybridization on the top and the bottom of the surface. As a consequence of this field, we assume a net ISB exchange energy $\mathcal{E}_z \neq 0$ acting on the atoms $\{a, b, d, e\}$ and the central atom $c$ does not take a role due to the fact that we still have $t_{bc} = t_{cd}$. Thus, we propose a new effective Hamiltonian from Eq. (1) as

$$\mathcal{H}_{\text{eff}}^{\text{ISB}}(\vec{k}) = \begin{pmatrix} \varepsilon_a & t_{ab}g_{\vec{k}} + \mathcal{E}_z & t_{ac}f_{\vec{k}}^* & 0 & t_{ae}f_{\vec{k}} \\ t_{ab}g_{\vec{k}}^* + \mathcal{E}_z & \varepsilon_b & t_{bc}g_{\vec{k}}^* & t_{bd}f_{\vec{k}}^* & 0 \\ t_{ac}f_{\vec{k}} & t_{bc}g_{\vec{k}} & \varepsilon_c & t_{cd}g_{\vec{k}} & t_{ce}f_{\vec{k}}^* \\ 0 & t_{bd}f_{\vec{k}} & t_{c}g_{\vec{k}}^* & \varepsilon_d & t_{de}g_{\vec{k}} + \mathcal{E}_z \\ t_{ae}f_{\vec{k}}^* & 0 & t_{ce}f_{\vec{k}} & t_{de}g_{\vec{k}}^* + \mathcal{E}_z & \varepsilon_e \end{pmatrix}. \quad (2)$$

## III. OPTICAL CONDUCTIVITY

In this section, we turn to the Kubo formula and the optical conductivity tensor $\sigma_{\alpha\beta}(\omega)$ of $\beta_{12}$-borophene based on the given Hamiltonian in Eq. (2). Within the linear-response theory framework, the Kubo conductivity reads [43]

$$\sigma_{\alpha\beta}(\omega) = i\sum_{\vec{k}}\sum_{\nu,\nu'} \frac{f_{\vec{k},\nu} - f_{\vec{k},\nu'}}{\mathcal{E}_{\vec{k},\nu} - \mathcal{E}_{\vec{k},\nu'}} \frac{\mathcal{J}_{\alpha\beta}^{\nu\nu'}(\vec{k})}{\hbar\omega + i\delta + \mathcal{E}_{\vec{k},\nu} - \mathcal{E}_{\vec{k},\nu'}}, \quad (3)$$

where $\nu$ and $\nu'$ stand for the band indices and $\{\alpha, \beta\} = \{x, y\}$ indicate different flavors. The Fermi-Dirac distribution function is given by $f_{\vec{k},\nu}$ and $\delta = 0.05$ eV is a small phenomenological factor which is responsible for controlling the width of optical peaks. The tensor current $\mathcal{J}_{\alpha\beta}^{\nu\nu'}(\vec{k}) = \langle\vec{k}, \nu|j_\alpha|\vec{k}, \nu'\rangle\langle\vec{k}, \nu'|j_\beta|\vec{k}, \nu\rangle$ can also be calculated via $j_\alpha = e\partial\mathcal{H}/\partial k_\alpha$. Taking into account the derivatives of Hamiltonian along both directions, we numerically obtain $j_x$ and $j_y$. The effect of the ISB field $\mathcal{E}_z$ is already induced to the energy bands and the Fermi-Dirac distribution functions in the above equation.

Having numerically both dispersion relations $\mathcal{E}_{\vec{k},\nu}$ and eigenstates $|\vec{k}, \nu\rangle$ of different bands, the optical conductivity can be calculated numerically. We set $\hbar = e = 1$ for simplicity throughout the paper. The fermions in the effective Hamiltonian model disperse along the $x$ and $y$ directions differently and this affects the $\vec{k}$-dependent current operators $\{j_x, j_y\}$. This is a direct result of the anisotropic band structure of $\beta_{12}$-borophene and this, in turn, leads to strongly anisotropic optical conductivity, i.e., $\sigma_{xx} \neq \sigma_{yy} \neq \sigma_{xy}$.

In this paper, we focus on the optical interband transitions and neglect the intraband ones since we assume that the momentum relaxation time approaches zero in the same bands at zero Fermi energy which is mostly valid for a clean sample at a low temperature of 8 to 10 K. Intraband transitions (which occur at low energies) are thye free-carriers process, and it is well known that the long-range correlations of electrons in the same conduction band are treated in terms of collective oscillations at the plasma frequency of the system, and this occurs if they contribute to the infrared absorption of free electrons as in the Drude model. In this model, the incident electromagnetic radiation of frequencies below the plasma frequency is reflected since the electrons in the metallic phase screen the electric field of the light wave, whereas above the plasma frequency, the radiation is transmitted because in this case, the electrons cannot respond fast enough to screen it. From these points, one would argue that the intraband transitions within the same band mainly contribute to the optical conductivity in the presence of the disorder or scattering in the terahertz or infrared region, which can be described as Drude-like conductivity. However, the small density of states in these regions cannot lead to weak intraband transitions, and mostly interband transitions following quantum-mechanical processes are dominant. So, the intraband transitions which only contribute to the peaks in the optical conductivity close to the zero photon energy are hard to be distinguished in the metallic phase since the low-energy region also includes the interband transitions from an occupied state below the Fermi level, to an unoccupied state in a higher band. Since we do not consider any disorder or scattering mechanism in the theory for the optical intraband transitions, we would stick to the interband ones which also contain enough information at very low energies of the band structure of $\beta_{12}$-borophene. For this reason, we should argue that the modulation of intraband transitions is qualitatively close to the changes made for the interband transitions with the ISB field.

## IV. NUMERICAL RESULTS AND DISCUSSION

Now let us discuss the results of our paper with the effects of the proposed ISB field. We divide the following results into two parts, the manipulation of anisotropic electronic band structure and interband optical transitions with the ISB field. We stress that the energy regime where the tight-binding model is in line with the experimental data [30,31] is only about 2 eV in $\beta_{12}$-borophene. We use this upper limit to

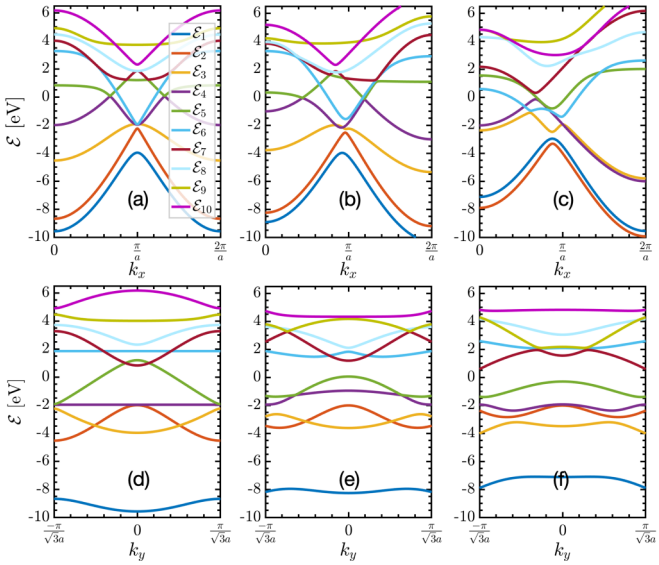


FIG. 3. Dispersion energy of $\beta_{12}$-borophene along the $x$ direction in the (a) absence and {(b) and (c)} presence of the ISB field $\mathcal{E}_z$. The same for (d) and {(e) and (f)} along the $y$ direction. The ISB field is $\mathcal{E}_z = 1$ and 2 eV for panels {(b) and (e)}, and {(c) and(f)}, respectively.

validate our results of the blueshift and redshift spectra because the tight-binding model based on density functional theory has already been well matched with the experimental observations for the metallic phase of $\beta_{12}$-borophene. This means that the ISB field is not far from the reality of the dispersion of fermions and would be covered by the band structure of the system.

### A. Electronic band structure

We start with the pristine $\beta_{12}$-borophene, Figs. 3(a) and 3(d), which shows a strong anisotropy feature since the fermions disperse differently along the $x$ and $y$ directions. In the pristine state of $\beta_{12}$-borophene, the electronic band structure consists of ten curves (the first five curves at $\vec{k} = 0$ and the other five curves at $\vec{k} \neq 0$) [30,31]. It should be noted that one only expects five bands from the Hamiltonian, i.e., we actually have five bands $E_1 = \{\mathcal{E}_1, \mathcal{E}_2\}$, $E_2 = \{\mathcal{E}_3, \mathcal{E}_4\}$, $E_3 = \{\mathcal{E}_5, \mathcal{E}_6\}$, $E_4 = \{\mathcal{E}_7, \mathcal{E}_8\}$, and $E_5 = \{\mathcal{E}_9, \mathcal{E}_{10}\}$ instead of ten individual curves at different momenta $\vec{k} = 0$ and $\vec{k} \neq 0$. But this helps to find the metallic nature of the system, first, and second to label the multi-interband optical transitions later. Along the $x$ direction, Fig. 3(a), the inversion symmetric model contains two Dirac cones at the zero Fermi energy level located at $\vec{k} = (2\pi/3a, 0)$, $\vec{k} = (-2\pi/3a, 0)$, and two triplet fermions located at $\vec{k} = (\pi/a, \pi/\sqrt{3}a)$ and $\vec{k} = (\pi/a, 0)$, respectively. The blue curve $\mathcal{E}_6$ and the Dirac cones are responsible for the metallic nature of $\beta_{12}$-borophene. However, along the $y$ direction, the green curve $\mathcal{E}_5$ is mainly responsible for the metallic phase, see Fig. 3(d).

As soon as we apply the ISB field, independent of the direction of the field, the electronic bands are manipulated and the inversion symmetry above mentioned is mainly broken such that at $\mathcal{E}_z = 1$ eV along the $x$ direction, Fig. 3(b), Dirac fermions are not dispersing symmetrically anymore, and the triplet fermions are partially destroyed. The destruction of triplet fermions means distributed contribution in other directions. These behaviors remove the flat bands along the $y$ direction and change the concavity of curves (change in the sign of effective mass of fermions) but do not affect the inversion symmetrical behavior of bands, Fig. 3(e). Subsequently, the $y$ direction, Fig. 3(f), still intends to show the inversion symmetry, however, a very interesting thing happens: two Dirac-like fermions appear from curves 7 and 9, and with this, optical interband transitions can be influenced significantly. If we look at the bands at the same ISB field along the $y$ direction, Fig. 3(e), we still observe an inversion symmetry. From the geometry structure of the system, Fig. 1, the structure factors $f_{\vec{k}}$ and $g_{\vec{k}}$ in Eq. (1) are conserved along the $y$ direction—armchair direction—and each centered ribbon is symmetric around the noncentered ribbon. Thus, the $y$ direction is strong against spatial symmetry-breaking fields, such as the ISB one here.

Considering $\mathcal{E}_z = 2$ eV in Fig. 3(c), compared to the dispersion of both pristine triplet and Dirac fermions along the $x$ direction shows that the system does not have any Dirac fermions anymore, whereas a new triplet fermion at a different momentum coordinate $0 < k_x < \pi/a$ is created among bands 4–6. Following this variation, the $y$ direction in Fig. 3(f) still keeps the previous setup of the band structure. All these changes in the electronic band structure of $\beta_{12}$-borophene in the presence of $\mathcal{E}$ will change the optical selection rules for the multi-interband transitions.

### B. Optical conductivity

As discussed before, we work with ten curves here to achieve the same metallic known phase of $\beta_{12}$-borophene. In general, due to the strong inherent anisotropy of the system, we, respectively, find ten, four, and three different types of interband transitions along the $x$ direction, $y$ direction, and on the plane of the system. The last one is called the Hall transition. The selection rules of the optical conductivity are not identical in different directions, and we use the labels of curves in Fig. 3(a) to determine the effective possible interband transitions. Having all partial contributions, the total optical conductivity is obtained.

For the real part of total optical conductivity along the $x$ direction, five peaks emerge at optical energies $\hbar\omega \simeq 1$, 1.5, 2.75, 3.25, and 4.75 eV, see the black curve of Fig. 4(a). Basically, we have transitions $\mathcal{E}_2 \mapsto \mathcal{E}_{5,6}$, $\mathcal{E}_3 \mapsto \mathcal{E}_{5,6,7,8}$, and $\mathcal{E}_4 \mapsto \mathcal{E}_{5,6,7,8}$. From the position of peaks, it is not hard to find out that: (i) the first peak is due to the optical transition between curves 4 and 6, (ii) the second peak is due to the transition between curves 4 and 7, (iii) the third peak is due to the transition from curve 4 to curves 5 and 8, (iv) the small fourth peak is due to the transition between curves 3 and 5, and (v) finally, the last fifth peak is a direct result of the transition of fermions between curves 2 and 5. It should be mentioned that only six types of transitions play a majority role in the total optical conductivity and the transitions $\mathcal{E}_2 \mapsto \mathcal{E}_6$, $\mathcal{E}_3 \mapsto \mathcal{E}_7$, and $\mathcal{E}_3 \mapsto \mathcal{E}_8$ take a negligible role in the total $\sigma_{xx}(\omega)$. The left transition is between bands 3 and 6 which together with the transition from band 4 to 5 is mainly contributed to the static

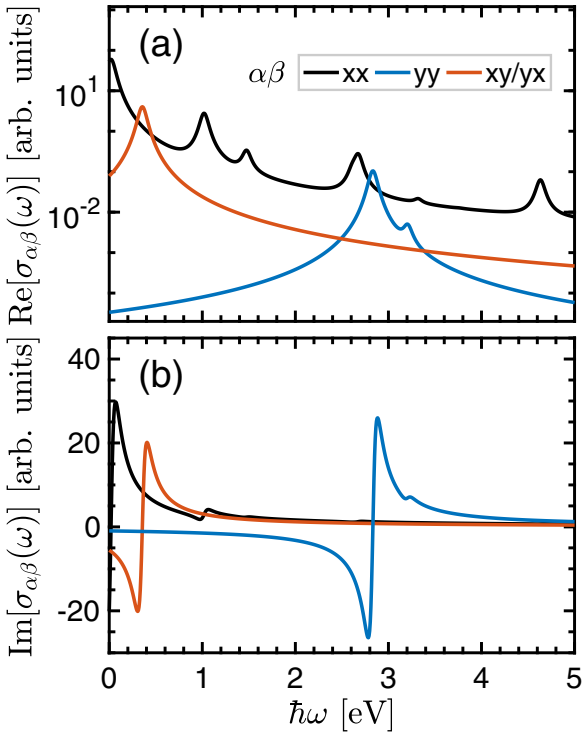


FIG. 4. (a) Real and (b) imaginary parts of the total pristine optical conductivity of $\beta_{12}$-borophene along different directions as a function of the photon energy. In both parts, the optical conductivity is almost zero for $\hbar\omega > 5$ eV.

conductivity at almost zero optical energy—Drude peak—and will be tuned with the ISB field later. On the other hand, the electronic band structure in Fig. 3(a) stresses that the static transition occurs if the distance between bands is almost zero.

Turning to the $yy$ component and the $xy/yx$ component of the optical conductivity tensor of the system, the effective interband transitions are $\mathcal{E}_2 \mapsto \mathcal{E}_7$ and $\mathcal{E}_4 \mapsto \mathcal{E}_{5,6,7}$ from Fig. 3(d) and based on our numerical results, the transition between curves {2,4} and 7 contribute mostly to the total conductivity. This transition leads to a peak at $\hbar\omega \simeq 2.8$ eV and a small peak at 3.4 eV in the real part of total optical conductivity, see the blue curve of Fig. 4(a). This, in turn, means that the other transitions between curves 4 and {5,6} show negligible effects. In the case of in-plane Hall conductivity $\sigma_{xy}(\omega)$ of $\beta_{12}$-borophene, the transitions $\mathcal{E}_{3x} \mapsto \mathcal{E}_{6y}$ and $\mathcal{E}_{4x} \mapsto \mathcal{E}_{5y,6y}$ are possible, however, the effective one is originated from $\mathcal{E}_{4x} \mapsto \mathcal{E}_{5y}$, leading to again a single peak at $\hbar\omega \simeq 0.25$ eV, see the orange curve of Fig. 4(a). And the two other transitions are negligible.

In all directions, one expects the same number of peaks at the same energy positions in the imaginary parts by following the Kramers-Kronig relation [44], see Fig. 4(b). In the following, we turn to the impact of the ISB field on the real part of optical conductivity and stop the imaginary part because the Kramers-Kronig relation works for both pristine and ISB field-induced $\beta_{12}$-borophene. By considering two different regimes of ISB fields 1 and 2 eV, the optical conductivity spectrum varies compared to the pristine case. The main reason can be understood from the fact that the concavity

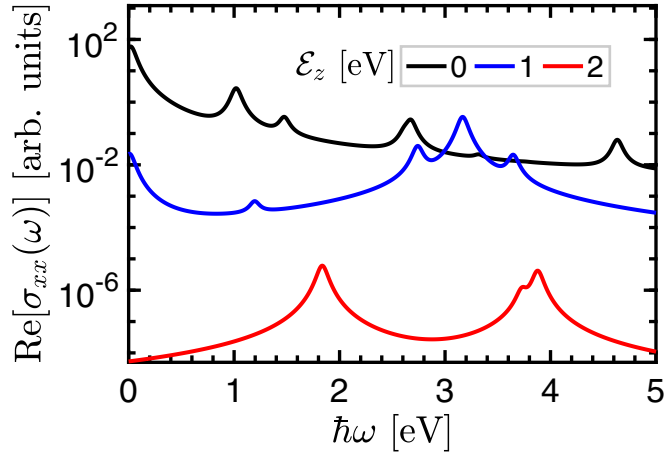


FIG. 5. The real part of the total ISB field-induced optical conductivity of $\beta_{12}$-borophene along the $x$ direction as a function of the light energy $\hbar\omega$. The system experiences a redshift spectrum.

of bands is changed with the ISB field which directly affects the propagating momentum.

#### *1. Longitudinal*

Let us start with the ISB-induced optical conductivity along the $x$ direction. Figure 5 shows that the five transition peaks mentioned before in the pristine case are no longer present as $\mathcal{E}_z$ is turned on since the propagation of incident light is changed with the ISB field. For $\mathcal{E}_z = 1$ eV in Fig. 5, one of the peaks disappears. Our investigation shows that the contribution of transition between curves 3 and {5, 6} and 4 and {5, 6} from the previous set still play significant roles. For the Drude conductivity, the transition from band 4 to 5 is important. They also form the third peak, whereas the first, second, and fourth peaks originate from the transition among curves {3 and 6}, {4 and 7}, and {3 and 5}, respectively. In this strength of the ISB field, we find the *redshift* spectrum for the system.

Increasing the ISB field to $\mathcal{E}_z = 2$ eV in Fig. 5 results in three peaks in which the second and third peaks mainly are originated from the transition between bands 3 and 5, whereas the transition $3 \mapsto 6$ occurs for the first peak. Similar to the previous strength of the ISB field, the redshift phenomenon occurs for $\mathcal{E}_z = 2$ eV.

#### *2. Transverse*

Now, we turn to the real part of the optical conductivity of ISB field-induced $\beta_{12}$-borophene along the $y$ direction in Fig. 6. As discussed before, the optical selection rules are different compared to the $x$ direction and the pristine transition between bands {2,4} and 7 is mainly responsible for the total $\sigma_{yy}(\omega)$. However, this argument is not valid with $\mathcal{E}_z = 1$ eV and four transitions between bands {4,5} and {6 and 7} emerge. The peaks, respectively, stem from $\mathcal{E}_5 \mapsto \mathcal{E}_6$, $\mathcal{E}_5 \mapsto \mathcal{E}_7$, $\mathcal{E}_4 \mapsto \mathcal{E}_6$, and $\mathcal{E}_4 \mapsto \mathcal{E}_7$. For the shift of peak, one can argue that the system experiences *the coexistence of both redshift and blueshift* phenomena appearing for $\mathcal{E}_z = 1$ eV along the $y$ direction which is new.

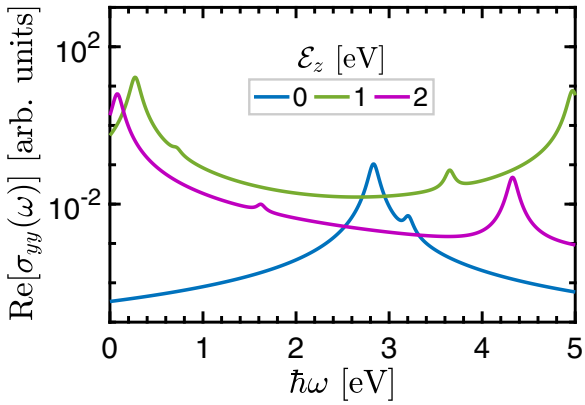


FIG. 6. The real part of the total ISB field-induced optical conductivity of $\beta_{12}$-borophene along the $y$ direction as a function of the light energy $\hbar\omega$. This time, the system experiences both redshift and blueshift spectra along the $y$ direction.

Similar to the $x$ direction, the ISB field of 2 eV along the $y$ direction behaves differently, see the red curve in Fig. 6. In this case, the effective optical transition leads to three peaks, one small peak at $\hbar\omega \simeq 1.6$ eV and two large peaks at $\hbar\omega \simeq 0.5$ and 4.3 eV. They, respectively, mainly are due to the transitions $\mathcal{E}_5 \mapsto \mathcal{E}_6$, $\mathcal{E}_5 \mapsto \mathcal{E}_7$, and $\mathcal{E}_5 \mapsto \mathcal{E}_9$ which the last one is a new type of transition compared to the pristine and weaker cases. All these transitions are again accompanied by simultaneous redshift and blueshift spectra but with lower intensity compared to the previous field.

#### *3. Hall conductivity*

Finally, we focus on the optical Hall conductivity in the plane of $\beta_{12}$-borophene when various ISB fields are applied. In the pristine phase, we observed a single low-frequency peak, whereas various peaks can be found when $\mathcal{E}_z$ is turned on. In Fig. 7, we start with $\mathcal{E}_z = 1$ eV, the blue curve for which a single peak still comes up at optical energy 2.5 eV. In contrast to the pristine transition $\mathcal{E}_{4x} \mapsto \mathcal{E}_{5y}$, the peak corresponds to the transition $\mathcal{E}_{4x} \mapsto \mathcal{E}_{7y}$ and the Drude peak corresponds to the transition $\mathcal{E}_{5x} \mapsto \mathcal{E}_{6y}$. For other ISB field of $\mathcal{E}_z = 2$ eV,

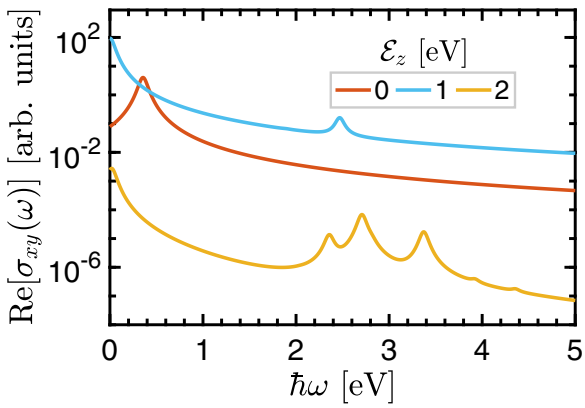


FIG. 7. The real part of the total ISB field-induced Hall conductivity of $\beta_{12}$-borophene as a function of the light energy $\hbar\omega$. The system experiences a blueshift spectrum on the plane of the lattice.

the red curve in Fig. 7, one obtains five peaks (at energies 2.3, 2.7, 3.4, 3.9, and 4.4 eV) corresponding to the optical transitions $\mathcal{E}_{5x} \mapsto \mathcal{E}_{8y}$, $\mathcal{E}_{5x} \mapsto \mathcal{E}_{7y}$, $\mathcal{E}_{4x} \mapsto \mathcal{E}_{7y}$, $\mathcal{E}_{4x} \mapsto \mathcal{E}_{9y}$, and $\mathcal{E}_{5x} \mapsto \mathcal{E}_{8y}$. Interestingly, the transition $\mathcal{E}_{5x} \mapsto \mathcal{E}_{6y}$ leads to the Drude peak. On the average, these ISB fields lead to a *blueshift* spectrum for $\beta_{12}$-borophene.

It is worthwhile commenting that the optical transitions can be influenced by doping the system through acceptor or donor atoms. On the one hand, it is well known that this can be controlled via the Fermi energy which depending on the type of doping can shift the electronic bands to higher and lower energies. On the other hand, our paper is strongly band dependent since the optical selection rules in the Kubo formula depend on the eigenvalues and eigenstates of particles in the system. Hence, the propagation of fermions and the concavity of bands cannot be affected qualitatively, and the same results are expected to appear for the optical properties of doped $\beta_{12}$-borophene when it is subjected to a light beam and an ISB field.

## V. CONCLUSIONS

We have investigated the electronic and optical properties of the $\beta_{12}$-borophene within the linear-response theory using the generalized tight-binding approximation whereas taking into account an ISB field in the framework of a perturbation method. $\beta_{12}$-borophene is naturally a metal that is characterized by central boron atoms located in the center of a honeycomb lattice. This atomic configuration explains the inversion symmetrical behavior of Dirac and triplet fermions in $\beta_{12}$-borophene. Despite the unique features of this system, this symmetry can be broken by an external proper field away from the central atoms, which results in the manipulation of the dispersion energy of the system. We have also investigated theoretically the effect of ISB field on the optical responses of $\beta_{12}$-borophene. In addition to the static Drude peak in the limit of zero frequency, the calculated pristine spectra along different directions possess multisharp optical interband transitions below 5 eV along the $x$ direction, whereas along the $y$ direction and on the plane of the lattice, one can find two transitions a single transition, respectively.

We have shown that there is a distinct phenomenology arising from the ISB field. In the presence of the ISB field, we find the coexistence of both redshift and blueshift spectra along the $y$ direction, whereas the $x$ direction (the $x$-$y$ plane) of the system leads to a pure redshift (blueshift) spectrum. We conclude that, unlike the pristine metallic phase of $\beta_{12}$-borophene, the ISB effects, which can occur due to an interaction with atomic substrates, can be relatively effective in modulation of physical properties of the low-dimensional systems, which, in turn, can be helpful in engineering the practical optoelectronic applications.

## ACKNOWLEDGMENT

M.Y. gratefully acknowledges financial support by the Welch Foundation through Award No. AT-2036-20200401.

[1] K. S. Novoselov, A. K. Geim, S. V. Morozov, D. Jiang, Y. Zhang, S. V. Dubonos, I. V. Grigorieva, and A. A. Firsov, Science **306**, 666 (2004).

[2] A. K. Geim, Science **324**, 1530 (2009).

[3] C.-C. Liu, H. Jiang, and Y. Yao, Phys. Rev. B **84**, 195430 (2011).

[4] M. Ezawa, Phys. Rev. Lett. **109**, 055502 (2012).

[5] M. Derivaz, D. Dentel, R. Stephan, M.-C. Hanf, A. Mehdaoui, P. Sonnet, and C. Pirri, Nano Lett. **15**, 2510 (2015).

[6] F.-F. Zhu, W.-J. Chen, Y. Xu, C.-L. Gao, D.-D. Guan, C.-H. Liu, D. Qian, S.-C. Zhang, and J.-F. Jia, Nature Mater. **14**, 1020 (2015).

[7] Y. Xu, B. Yan, H.-J. Zhang, J. Wang, G. Xu, P. Tang, W. Duan, and S.-C. Zhang, Phys. Rev. Lett. **111**, 136804 (2013).

[8] A. Splendiani, L. Sun, Y. Zhang, T. Li, J. Kim, C.-Y. Chim, G. Galli, and F. Wang, Nano Lett. **10**, 1271 (2010).

[9] C. Kamal, A. Chakrabarti, and M. Ezawa, New J. Phys. **17**, 083014 (2015).

[10] C. Kamal and M. Ezawa, Phys. Rev. B **91**, 085423 (2015).

[11] S. Zhang, Z. Yan, Y. Li, Z. Chen, and H. Zeng, Angew. Chem., Int. Ed. **54**, 3112 (2015).

[12] I. K. Drozdov, A. Alexandradinata, S. Jeon, S. Nadj-Perge, H. Ji, R. J. Cava, B. Andrei Bernevig, and A. Yazdani, Nat. Phys. **10**, 664 (2014).

[13] L. Li, Y. Yu, G. J. Ye, Q. Ge, X. Ou, H. Wu, D. Feng, X. H. Chen, and Y. Zhang, Nat. Nanotechnol. **9**, 372 (2014).

[14] H. Liu, A. T. Neal, Z. Zhu, Z. Luo, X. Xu, D. Tománek, and P. D. Ye, ACS Nano **8**, 4033 (2014).

[15] F. Xia, H. Wang, and Y. Jia, Nat. Commun. **5**, 4458 (2014).

[16] I. Boustani, Surf. Sci. **370**, 355 (1997).

[17] M. H. Evans, J. D. Joannopoulos, and S. T. Pantelides, Phys. Rev. B **72**, 045434 (2005).

[18] H. Tang and S. Ismail-Beigi, Phys. Rev. Lett. **99**, 115501 (2007).

[19] X. Wu, J. Dai, Y. Zhao, Z. Zhuo, J. Yang, and X. C. Zeng, ACS Nano **6**, 7443 (2012).

[20] E. S. Penev, S. Bhowmick, A. Sadrzadeh, and B. I. Yakobson, Nano Lett. **12**, 2441 (2012).

[21] H. Liu, J. Gao, and J. Zhao, Sci. Rep. **3**, 3238 (2013).

[22] Y. Liu, E. S. Penev, and B. I. Yakobson, Angew. Chem. Int. Ed. **52**, 3156 (2013).

[23] Z. Zhang, Y. Yang, G. Gao, and B. I. Yakobson, Angew. Chem. Int. Ed. **54**, 13022 (2015).

[24] C. Özdoğan, S. Mukhopadhyay, W. Hayami, Z. B. Güvenç, R. Pandey, and I. Boustani, J. Phys. Chem. C **114**, 4362 (2010).

[25] B. Mortazavi, O. Rahaman, S. Ahzi, and T. Rabczuk, Appl. Mater. Today **8**, 60 (2017).

[26] B. Mortazavi, A. Dianat, O. Rahaman, G. Cuniberti, and T. Rabczuk, J. Power Sources **329**, 456 (2016).

[27] X. Zhang, J. Hu, Y. Cheng, H. Y. Yang, Y. Yao, and S. A. Yang, Nanoscale **8**, 15340 (2016).

[28] B. Feng, J. Zhang, Q. Zhong, W. Li, S. Li, H. Li, P. Cheng, S. Meng, L. Chen, and K. Wu, Nat. Chem. **8**, 563 (2016).

[29] B. Feng, J. Zhang, R.-Y. Liu, T. Iimori, C. Lian, H. Li, L. Chen, K. Wu, S. Meng, F. Komori, and I. Matsuda, Phys. Rev. B **94**, 041408(R) (2016).

[30] M. Ezawa, Phys. Rev. B **96**, 035425 (2017).

[31] B. Feng, O. Sugino, R.-Y. Liu, J. Zhang, R. Yukawa, M. Kawamura, T. Iimori, H. Kim, Y. Hasegawa, H. Li, L. Chen, K. Wu, H. Kumigashira, F. Komori, T.-C. Chiang, S. Meng, and I. Matsuda, Phys. Rev. Lett. **118**, 096401 (2017).

[32] P. T. T. Le, T. C. Phong, and M. Yarmohammadi, Phys. Chem. Chem. Phys. **21**, 21790 (2019).

[33] B. D. Hoi, L. V. Tung, P. T. Vinh, D. Q. Khoa, and L. T. T. Phuong, Phys. Chem. Chem. Phys. **23**, 2080 (2021).

[34] H. T. T. Nguyen, B. D. Hoi, T. V. Vu, P. V. Nham, and N. T. T. Binh, Phys. Chem. Chem. Phys. **22**, 6318 (2020).

[35] D. Q. Khoa, N. N. Hieu, and B. D. Hoi, Phys. Chem. Chem. Phys. **22**, 286 (2020).

[36] L. Adamska and S. Sharifzadeh, ACS Omega **2**, 8290 (2017).

[37] A. Lherbier, A. R. Botello-Méndez, and J.-C. Charlier, 2D Mater. **3**, 045006 (2016).

[38] B. Peng, H. Zhang, H. Shao, Y. Xu, R. Zhang, and H. Zhu, J. Mater. Chem. C **4**, 3592 (2016).

[39] A. Mogulkoc, Y. Mogulkoc, D. Kecik, and E. Durgun, Phys. Chem. Chem. Phys. **20**, 21043 (2018).

[40] Y. Zhang, K. He, C.-Z. Chang, C.-L. Song, L.-L. Wang, X. Chen, J.-F. Jia, Z. Fang, X. Dai, W.-Y. Shan, S.-Q. Shen, Q. Niu, X.-L. Qi, S.-C. Zhang, X.-C. Ma, and Q.-K. Xue, Nat. Phys. **6**, 584 (2010).

[41] C.-X. Liu, H. Zhang, B. Yan, X.-L. Qi, T. Frauenheim, X. Dai, Z. Fang, and S.-C. Zhang, Phys. Rev. B **81**, 041307(R) (2010).

[42] X. Liu, Q. Li, Q. Ruan, M. S. Rahn, B. I. Yakobson, and M. C. Hersam, Nat. Mater. **21**, 35 (2022).

[43] G. Mahan, *Many-Particle Physics*, Physics of Solids and Liquids (Springer, New York, 2000).

[44] R. d. L. Kronig and H. A. Kramers, Z. Phys. **48**, 174 (1928).